Ring puckering landscapes of glycosaminoglycan-related monosaccharides from molecular dynamics simulations

Irfan Alibay[†,‡] and Richard A. Bryce[†*]

† Division of Pharmacy and Optometry, School of Health Sciences, University of Manchester, Oxford Road, M13 9PL, UK

‡ Structural Bioinformatics and Computational Biochemistry Unit, Department of Biochemistry, University of Oxford, South Parks Road, Oxford, OX1 3QU, UK

Corresponding Author

*Richard Bryce, Division of Pharmacy and Optometry, School of Health Sciences, University of Manchester, Manchester, M13 9PT, U.K. Email: R.A.Bryce@manchester.ac.uk, Tel: (0)161-275-8345, Fax: (0)161-275-2481; ORCID 0000-0002-8145-2345

Abstract

The conformational flexibility of the glycosaminoglycans (GAGs) are known to be key in their binding and biological function, for example in regulating coagulation and cell growth. In this work, we employ enhanced sampling molecular dynamics simulations to probe the ring conformations of GAG-related monosaccharides, including a range of acetylated and sulfated GAG residues. We first perform unbiased MD simulations of glucose anomers and the epimers glucoronate and iduronate. These calculations indicate that in some cases, an excess of 15 μs are required for adequate sampling of ring pucker due to the high energy barriers between states. However, by applying our recently developed msesMD simulation method (multidimensional swarm enhanced sampling molecular dynamics), we were able to quantitatively and rapidly reproduce these ring pucker landscapes. From msesMD simulations, the puckering free energy profiles were then compared for eleven monosaccharides found in GAGs; this includes to our knowledge the first simulation study of sulfation effects on GalNAc ring puckering. For the force field employed, we find that in general the calculated pucker free energy profiles for sulfated sugars were similar to the corresponding unsulfated profiles. This accords with recent experimental studies suggesting that variation in ring pucker of sulfated GAG residues is primarily dictated by interactions with surrounding residues rather than by intrinsic conformational preference. As an exception to this, however, we predict that 4-O-sulfation of GalNAc leads to reduced ring rigidity, with a significant lowering in energy of the $^{1}C_{4}$ ring conformation; this observation may have implications for understanding the structural basis of the biological function of GalNAc-containing glycosaminoglycans such as dermatan sulfate.

Introduction

Carbohydrates fulfil a wide range of key functions in nature, from energy sources and structural units to mediators of biomolecular recognition.[1] Pyranose ring puckering plays an important role in the structure-activity relationship of many carbohydrates. For example, the glycosaminoglycan (GAG) heteropolysaccharides play a major role in cell adhesion and profileration.[2,3] Their constituent hexose or hexuronic acid residues are often sulfated, interacting in a specific way with the basic residues of receptor proteins.[4,5] Furthermore, these pyranose rings have been observed to adopt non-chair ring conformations on binding: for example, L-iduronic residues of the anticoagulant GAG, heparin, adopt a skew-boat $^{2}S_{O}$ ring pucker and is essential in heparin activation of antithrombin III.[6]

However, to characterize the ring puckering free energy landscape of carbohydrates is non-trivial: it is challenging to study by NMR methods due to the microsecond timescale of pucker transitions and the low population of rare but important pucker states;[7,8] it is also difficult to examine ring puckering computationally due to the high energy barriers separating stable conformers, necessitating multi-microsecond molecular dynamics (MD) simulations.[9] Consequently, enhanced sampling MD techniques have been applied to the challenge of exploring carbohydrate ring pucker; this includes the adaptive reaction coordinate force method,[10] metadynamics[11-13] and replica exchange-based schemes.[14-17] To date, however, enhanced sampling MD methods have not been deployed to examine the ring puckering of GAG monosaccharides. Recently, we introduced the msesMD method (multi-dimensional swarm enhanced sampling molecular dynamics) as an intuitive and effective biased MD approach.[18] The msesMD method involves the coupling of a swarm of simulation replicas via attractive and repulsive potentials acting on dihedral angles of interest.[18-20] We demonstrated the computational efficiency of msesMD simulations in sampling Lewis tri- and tetrasaccharide

conformations separated by high energy barriers to rotation about glycosidic torsions.[18]

In this work, we apply msesMD simulations to characterize the free energy landscape of ring pucker in GAG-related monosaccharides. We first validate the msesMD approach against unbiased multi-microsecond MD simulations for four unmodified monosaccharides: the anomers, α-D-glucose (α-Glc) and β-D-glucose (β-Glc); and the uronic acid epimers, α-L-iduronic acid (IdoA) and β-D-glucuronic acid (GlcA). Having established the efficient and quantitative sampling of ring pucker populations for these monosaccharides by msesMD simulations, we then employ this method to study a range of N-acetylated and sulfated GAG residues of IdoA, GlcA, N-acetylglucosamine (GlcNAc) and N-acetylgalactosamine (GalNAc) (Figure 1). This work represents to our knowledge the first use of an enhanced sampling MD method to examine the puckering landscapes of sulfated monosaccharides, residues which feature in biologically key GAGs such as heparan sulfate/heparin, dermatan sulfate and chondroitin sulfate.[21-23]

Computational Methods

System preparation. All monosaccharide-water systems were built using the *tleap* module in AmberTools14.[24] Carbohydrate parameters were obtained from the GLYCAM 06 (version j-1) force field,[25] with additional parameters for the unsubstituted and N-sulfated glucosamine units obtained from a separate GLYCAM 06 release for glycosaminoglycan monosaccharides.[26] O-sulfated glycosaminoglycan monosaccharide parameters were set using the Glycam06 transferable sulfation method as described by Singh et al.[26] The various monosaccharides (Figure 1) were built in the $^4C_1$ ring configuration, with hydroxyl substituents at the C1 position. The systems were neutralised using sodium ions where appropriate and explicitly solvated in truncated octahedron boxes using TIP3P[27] waters placed a minimum of

13 Å away from the solute.

MD simulations. All simulations were equilibrated using the following protocol. Solvated monosaccharide boxes were minimised and then heated from 0 to 298 K over 500 ps under constant volume conditions (NVT). The box density was then equilibrated to a target pressure of 1 bar via 1 ns of constant pressure (NPT) simulation using the Monte Carlo barostat,[28] with volume exchange attempts every 100 steps. The system was then further equilibrated under NVT conditions for a further 1 ns. All subsequent simulations were carried out in the NVT ensemble.

Temperature control was achieved using the Langevin thermostat,[28,29] with a collision frequency of 3 ps^{-1} and a target temperature of 298 K. Hydrogen bond motion was constrained using the SHAKE[30] and SETTLE[31] algorithms for solute and water molecule respectively. A 2 fs integration timestep was used for all msesMD simulations, whilst the unbiased MD simulations employed the hydrogen mass repartitioning (HMR)[32] methodology with a timestep of 4 fs. Following Hopkins et al.,[33] 2 amu was repartitioned from heavy atoms to hydrogens via the AMBER *parmed* utility. A 9 Å cut-off was used for short range non-bonded interactions, with long range electrostatics calculated via the particle mesh Ewald approach.[34,35] Starting from the equilibrated systems, individual production simulations were propagated for a total of 10 μs, with configurations sampled every 5 ps. For α-Glc and GlcA, simulations were extended by a further 10 μs due to poor sampling of chair interconversion events.

msesMD simulations. The same overall msesMD simulation approach employed in our recent work was used here.[18] Briefly, eight replicas were coupled using our previously published swarm biasing potential with the parameters A = 3.195 kcal mol^{-1}, B = 2.625 rad^{-1}, C = 0.75

kcal mol^{-1} and D = 0.5 rad^{-1}. For all monosaccharides, the msesMD potential was applied to two non-overlapping ring torsions, O5-C1-C2-C3 and C3-C4-C5-O5. These boost coordinates were chosen due to their successful previous use in Hamiltonian replica exchange studies of uronic acid puckering by Babin and Sagui.[14] It is however noted that other puckering coordinates, such as Hill-Reilly[36] or Cremer-Pople angles,[37] have also been found to be effective in previous enhanced sampling studies[10,11] and could equally have been employed in the current work. On completing the unbiased MD equilibration process, eight independent trajectories were propagated over a 1 ns period. The msesMD potential was then slowly introduced across the replicas over a 600 ps period and the system allowed to re-equilibrate for a further 5.4 ns under the full influence of the potential. This was then followed by 195 ns per replica of production simulation with configurations sampled every picosecond.

Analysis. Cremer-Pople θ and ϕ angles were calculated to characterise monosaccharide pucker. To quantify differences in occupation of ring conformations ($^1C_4$, $^4C_1$, half-chair/envelope and boat/skew-boat), free energy surfaces were computed both as a function of θ and of θ and ϕ. For this, the relative Helmholtz free energy ΔA was computed from the normalised microstate probability density ρ_x according to $\Delta A = -k_B T \ln \rho_x$, where k_B is the Boltzmann constant and T is temperature. Estimates for ρ_x were obtained via the "counting approach" for unbiased MD simulations,[38] and for msesMD through the approach of Torrie and Valleau[39] as detailed previously.[18,20] A histogram bin size of 6° was used, with maximum energy cutoffs of 12 and 8 kcal/mol for the 1D and 2D surfaces respectively. Relative free energies of different puckering states, as shown in Tables 1 and 2, are presented as the lowest free energy bin value in the 2D Cremer-Pople θϕ range defining that particular puckering state. Ensemble average estimate errors for the msesMD simulations were calculated via bootstrap analysis, randomly resampling the simulation data 100,000 times and calculating the error as the standard deviation

in the bin energy estimates across all resamples.[18] These analyses were performed via in-house python scripts, using NumPy (www.numpy.org) and SciPy libraries (www.scipy.org); and the *cpptraj* program from AmberTools16.[40]

Results and discussion

Comparison of puckering free energy landscapes via MD and msesMD

Firstly, we compute the puckering free energy profiles for four biological relevant and computationally well-studied monosaccharides, α-Glc, β-Glc, IdoA and GlcA (Figure 1).[7,13,14,41] These pucker profiles (Figure 2) were computed as a function of Cremer-Pople angle θ, a coordinate which describes the change in conformation from the $^4C_1$ chair (θ = 0°) through boat/skew-boat (θ = 90°) to the $^1C_4$ chair pucker (θ = 180°). Unbiased MD studies of ring puckering in monosaccharides have previously suggested that simulation lengths of 5 - 10 μs are necessary to achieve converged puckering free energy profiles.[9,21] Interestingly, here we observe that explicit solvent MD simulations in excess of 15 μs were required to obtain a converged computed free energy profile of α-Glc (Figure 2a). Examination of the sampling of the θ pucker angle (Figure 3a) indicates infrequent transitions between the preferred $^4C_1$ chair and the higher energy $^1C_4$ (θ ~170°) states, via the boat/skew-boat pucker region at θ values of ~90°. The computed profiles for β-Glc and IdoA are broadly similar to that of α-Glc (Figure 2b,c); however, more frequent transitions to the $^1C_4$ pucker are exhibited for these monosaccharides (Figure 3c,e). For GlcA, the computed barrier to the $^1C_4$ pucker seems highest of the four monosaccharides (Figure 2d), with only two transient excursions to this conformation over the 20 μs trajectory (Figure 3g).

Despite the infrequent sampling of the $^1C_4$ state, there is reasonable agreement in the glucose

$^4C_1/^1C_4$ energy preference computed here with previous enhanced sampling MD studies. From our 20 μs unbiased MD simulations, the computed pucker landscapes indicate that for both α-Glc and β-Glc, the expected $^4C_1$ chair conformer is favored (Figure 2a,b); the $^4C_1$ preference is computed as 3.5 kcal/mol for β-Glc, but only 0.2 kcal/mol for the α-anomer (Table 1). This 3.3 kcal/mol reduction in preference by α-Glc for the $^4C_1$ pucker is reflected by other simulation studies: metadynamics simulations of glucose anomers,[10] using a reparameterised GROMOS 45a4 force field,[42] found a reduced $^4C_1$ preference for α-Glc by ~2.5 kcal/mol. A MD study[15] using replica exchange with solute tempering/bond softening (REST/BOS) in conjunction with the OPLS3[43] and SPC force fields, also found a reduction in stabilisation of $^4C_1$ for α–Glc by 2.2 kcal/mol, to the extent of $^1C_4$ being the preferred state for the α-anomer.

Our unbiased MD simulations predict the $^4C_1$ and $^1C_4$ forms of IdoA are also similar in energy, with a preference for $^1C_4$ of 0.3 kcal/mol (Figure 2c, Table 1). This is in accord with the observation of lability in IdoA ring pucker observed from previous MD simulation and NMR of the methyl aglycone.[9] For GlcA, the C5 epimer of IdoA, MD simulation predicts $^4C_1$ chair as the dominant ring pucker conformation (Figure 2d), by 2.8 kcal/mol over the inverted chair structure (Table 1).

We next turn to consider ring pucker profiles for the four monosaccharides computed using msesMD enhanced sampling simulations. Free energy landscapes were determined based on msesMD simulation lengths of 45, 95, 145 and 195 ns (Figure 4); good convergence was found by 145 - 195 ns; the slowest to converge was, perhaps not unexpectedly, the α-Glc puckering profile (Figure 4a). Bootstrap sampling analysis of these 1D free energy profiles from 195 ns msesMD simulations (Supporting Information, Figure S1) indicates errors lying well within 0.2 kcal/mol, although on occasion ranging up to 0.5 kcal/mol for very high energy half-chair

and envelope transitional conformers. Overall, however, the free energy profiles recovered from the msesMD simulations appear well converged.

Based on the 195 ns msesMD simulations, the free energy landscapes for the pucker conformations agree closely with the most exhaustive of the multi-microsecond unbiased MD simulations (Figure 2). For example, the profile of α-Glc captures the relatively small 0.2 kcal/mol preference for the $^4C_1$ form (Figure 2a, Table 1) that was predicted by the 15 and 20 μs MD simulations but not 1, 5 and 10 μs MD trajectories. The msesMD simulation of IdoA also correctly depicts a puckering free energy surface with a slight favoring of the $^1C_4$ conformer (Figure 2c). For the four sugars, agreement in the $^4C_1/^1C_4$ energy difference between unbiased MD and msesMD simulations differs by at most 0.4 kcal/mol; this highest deviation is found for GlcA (Table 1, Figure 2d). Indeed, the GlcA profile contains a high energy barrier of ~10 kcal/mol between boat/skew-boat forms and $^1C_4$ (Figure 2d). Modelling the GlcA pucker profile appears to pose a challenge for the unbiased simulations; as described above, the $^1C_4$ chair conformation region is only sampled twice for a few nanoseconds over the duration of the 20 μs MD simulation (Figure 3g). This contrasts with comprehensive sampling by msesMD replicas over the 195 ns simulation (Figure 3h).

To examine in more detail non-chair puckering states, we resolve the puckering free energy surface according to both Cremer-Pople angles, θ and ϕ. As for the free energy profiles based solely on θ, the θϕ puckering profiles from msesMD have low bootstrap errors (Figure S2) and are in good agreement with unbiased MD predictions (Figure 5). The differing boat/skew-boat populations of the four monosaccharides on the puckering hypersurface is evident and reproduced by msesMD (Figure 5). The predicted identity of the lowest lying non-chair conformer agrees well in all four cases (Table 1). Interestingly, the epimers IdoA and GlcA

exhibit a marked difference in preferred intermediate conformer, switching from $^{2}S_{O}$ for IdoA (Figure 5e,f) to $^{1}S_{3}$ for GlcA (Figure 5g,h; Table 1). The ability of IdoA to readily access the $^{2}S_{O}$ conformer has been observed in previous MD simulations and NMR of hexasaccharide models of heparan sulfate.[22]

For each of the four monosaccharides, the relative free energy of the lowest lying non-chair conformer from MD and msesMD agrees to within 0.2 kcal/mol (Table 1). The exception is for α-Glc, where a difference of 0.5 kcal/mol is found between MD and msesMD estimates for $^{1}S_{5}$ (Table 1), a conformer which lies in the θϕ region of (90°, 250-300°). In overall terms, however, there is good agreement between multi-microsecond MD and msesMD methods in predicted θ and θϕ free energy profiles for ring puckering of α-Glc, β-Glc, IdoA and GlcA. The detailed shifts in populated puckering states as a function of anomer and epimer are reproduced.

Effect of sulfation on puckering free energy landscape

Based on this assessment, we next apply our msesMD simulations to evaluate the pucker profiles of eleven biologically relevant sulfated monosaccharides derived from the IdoA, GlcA, β-Gal and β-Glc residues. As before, an assessment of convergence in the free energy profiles computed by the msesMD simulations was performed; for the eleven systems, the pucker free energy profiles typically had converged to within 0.2 kcal/mol by 195 ns (Figures S3-S5), with bootstrap errors also generally on the order of 0.2 kcal/mol (Figures S6-S11).

We first consider the 2-O-sulfated forms of IdoA and GlcA, residues commonly found in GAGs; these are denoted IdoA2S and GlcA2S respectively (Figure 1). The ring pucker profiles computed from 195 ns msesMD simulations predict that 2-O-sulfation of IdoA produces a

subtle switch in preference (Figure 6a), from a free energy difference of 0.5 kcal/mol favoring the $^{1}C_{4}$ form over $^{4}C_{1}$ in IdoA; to a 0.2 kcal/mol preference for the $^{4}C_{1}$ over $^{1}C_{4}$ pucker in IdoA2S (Table 1). In addition, there is stabilisation of the two main skew-boat forms, $^{3}S_{1}$ and $^{2}S_{O}$ (Figure 7a,b): on sulfation, the relative free energy of $^{2}S_{O}$ is lowered from 1.5 to 1.3 kcal/mol, although we note this 0.2 kcal/mol difference lies within error (Tables 1 and 2). For $^{3}S_{1}$, the relative free energy is reduced from 1.7 to 1.1 kcal/mol on sulfation. As mentioned above, the $^{2}S_{O}$ conformation of the IdoA2S residue is significant, with NMR indicating this pucker is adopted by oligosaccharides that bind antithrombin III, including heparin.[44,45]

For 2-O-sulfation of GlcA, there is a smaller effect on pucker distribution, for the chair forms (Figure 6b) and for the intermediate boat/skew-boat populations (Figure 7c,d). For both GlcA and GlcA2S, the $^{1}S_{3}$ and $B_{O,3}$ structures lie within 2.4 kcal/mol of the lowest energy $^{4}C_{1}$ conformation and are more favored than the $^{1}C_{4}$ conformer (Tables 1 and 2). The substitution of the O2 hydroxyl in GlcA with a bulkier O-sulfate in GlcA2S might be expected to lead to a decrease the $^{1}C_{4}$ population, as the O2 group is in the axial orientation in the latter case. However the 0.6 kcal/mol increase in stability of the $^{1}C_{4}$ pucker on sulfation appears to arise from the compensating presence in msesMD simulations of hydrogen bonding between the O4 hydroxyl of GlcA2S and its axial 2-O-sulfate group (data not shown).

We consider next the hexosamine GlcNAc, the most widely modified GAG monomer in nature, and four of its commonly occurring variants (Figure 1): firstly, from N-deacetylation and subsequent N-sulfation of GlcNAc, the N-sulfo glucosamine (GlcNS) is obtained. GlcNS can undergo further O-sulfation through the action of heparan sulfate sulfotransferases at either the O3, O6 or both positions, leading to GlcNS(3S), GlcNS(6S) and GlcNS(3S,6S) residues respectively (Figure 1).

For all five compounds, a similar free energy dependence on pucker angle θ is predicted by the 195 ns msesMD simulations (Figure 6c); these profiles indicate a distinct preference for the $^4C_1$ chair form in all cases. For GlcNAc, a preference for the $^4C_1$ over $^1C_4$ conformation is computed here as 1.4 kcal/mol (Table 2); this energy difference was estimated as 3.5 kcal/mol from previous analysis of two 10 μs MD simulations of GlcNAc using the GLYCAM 06 force field.[23] Accessible from this $^4C_1$ minimum are a range of boat/skew-boat forms at $\theta \approx 90°$ via a barrier of ~8 kcal/mol (Figure 6c). Here, resolving the equatorial pseudorotation region obtained by msesMD simulation finds a diverse range of boat/skew-boat conformations (Figure 7e-i), with the most stable conformers occupying energies ranging from 3.6 – 4.4 kcal/mol from the $^4C_1$ minimum (Table 2). A similar range of boat and skew-boat conformers were obtained from the 2 x 10 μs MD study.[21] Nevertheless, sampling the complex puckering landscape of sulfated GlcNAc systems is challenging[21,46] and in that same study, 2 x 10 μs MD simulations of GlcNS(3S) and GlcNS(3S,6S) observed no $^4C_1$-to-$^1C_4$ transitions, and for the GlcNS(6S) residue, one transition was observed.[21] Here, we observe frequent sampling over the pucker coordinate, leading to computation of a continuous puckering free energy surface across θ (Figure 6c); we do note, however, that not all replicas of the swarm sampled the complete range of θ (Figure S13).

Finally, we consider the ring pucker of hexosamine, GalNAc, and three of its derivatives found in GAGs: these are sulfated at the O4, O6 or both these positions in GalNAc, and are denoted GalNAc(4S), GalNAc(6S) and GalNAc(4S,6S) respectively (Figure 1). Relatively little work has been performed computationally or experimentally on the study of GalNAc ring pucker,[46] and to our knowledge, no work exists on the effect of its O-sulfation. As for GlcNAc and its derivatives, we find here that msesMD simulation of the four GalNAc-based monosaccharides

exhibit a strong preference for the $^4C_1$ chair conformer (Figure 6d). The predicted barrier to accessing the boat/skew-boat region is also similar to that of GlcNAc, with a value of ~7 kcal/mol (Figure 6d).

Here, however, the comparison with GlcNAc ends: this boat/skew-boat region of GalNAc and its sulfated forms appears restricted to the $^1S_3$ skew-boat pucker (Figure 7j-m), as opposed to the more diverse range of structures accessible to GlcNAc and its derivatives (Figure 7e-i). Based on the msesMD simulations, the computed stability of the $^1S_3$ form is between 3.5 and 4.4 kcal/mol lower than that of the $^4C_1$ minimum of GalNAc and its derivatives (Table 2). Most striking however is the lack of stability of its $^1C_4$ form. Indeed, the lowest energy $^1C_4$ structures are found for GalNAc(4S) and GalNAc(4S,6S), which lie 5.0 and 8.3 kcal/mol above the $^4C_1$ form respectively. A previous 5 μs MD simulation of GalNAc in explicit aqueous solvent[46] observed the inaccessibility of the $^1C_4$ form, unable to sample any of that conformer over the duration of these simulations. Similarly, no $^1C_4$ conformer is sampled for GalNAc and GalNAc(6S) by msesMD simulations here, although it is sampled in the other sulfated forms (Figure S14).

In terms of the physical origin of these observations, we note that a $^4C_1$-to-$^1C_4$ transition for GalNAc involves displacing four of its ring substituents from equatorial to axial positions; this leads to unfavorable 1,3-diaxial interactions in the $^1C_4$ structure of GalNAc. Introduction of sulfation at the O6 position only compounds this effect. Conversely, msesMD simulation predicts that O4 sulfation of GalNAc significantly stabilises its $^1C_4$ pucker, such that it lies at 5 kcal/mol above the $^4C_1$ chair (Table 2). This is in part due to the bulky O4 sulfate group occupying a strained axial position in the $^4C_1$ chair, thus shifting the conformational equilibrium towards $^1C_4$. The $^1C_4$ form is also stabilised by formation of intra-ring hydrogen

bonding between the sulfate and hydroxyls groups in GalNS(4S) (Figure 8a); for GalNS(4S,6S), intra-ring hydrogen bonding is also observed (Figure 8b). However for this monosaccharide, minimizing electrostatic repulsion between sulfate groups is an additional factor governing ring conformation.

Conclusions

In this work, we explore the ring puckering landscape of thirteen glycosaminoglycan monosaccharides using enhanced sampling molecular dynamics simulations via the msesMD method. We first demonstrate that msesMD efficiently probes the thermodynamics of pyranose rings for four monosaccharides. At an order of magnitude lower computational cost, the application of a swarm biasing potential to two ring dihedrals via msesMD yielded puckering free energy profiles for the four monosaccharides in quantitative agreement with long timescale MD simulations. In the cases of α–Glc and GlcA, unbiased MD simulations over 15 μs in length were required for adequate sampling; thus, some monosaccharides appear to require longer simulation times than previously thought.[9,21] For the msesMD simulations, we also note that the parameters for the swarm biasing potential employed in this work are the same as used in previous efficient sampling of glycosidic and peptide backbone torsional degrees of freedom,[20] suggesting a degree of transferability in this biasing potential.

We then applied msesMD simulations to compare the puckering free energy landscapes for eleven glycosaminoglycan monosaccharides: we find that for sulfated and unsulfated forms of IdoA, GlcA, GlcNAc and, to a lesser degree, GalNAc, the free energy profiles are rather similar. For IdoA and IdoA2S, an NMR analysis of eight heparin sulfate-based hexasaccharides concluded that the variation in $^{4}C_{1}$:$^{2}S_{O}$:$^{1}C_{4}$ populations of the IdoA/IdoA2S residue was dictated by the differing sulfation patterns of *neighbouring* residues.[22] This suggests that inter-

residue hydrogen bonds and other interactions arising from the interplay of sulfated and non-sulfated groups play a key role in dictating shape and function of GAG polysaccharides.

Secondly, our msesMD study of GalNAc derivatives found that, although the galactosamine ring was more rigid than for GlcNAc, 4-O-sulfation of GalNAc led to a somewhat unexpected stabilisation of the $^{1}C_{4}$ form and lowering of the energy barrier leading to this conformer (Figure 6d). Although still predicted as 5.0 kcal/mol higher in energy than the $^{4}C_{1}$ conformer, the potential access to a $^{1}C_{4}$ form could be relevant to the structure, interaction and function of polysaccharides such as dermatan sulfate. The anticoagulant activity of dermatan sulfate from *Ascidian nigra*, possessing 6-O-sulfated GalNAc residues, has been examined;[47] this was compared with the activity of the mammalian form, which contains solely 4-O-sulfated GalNAc. It was found that only the mammalian form exhibited anticoagulant activity and potent interaction with heparin cofactor II. This suggests that 4-O-sulfation of GalNAc residues is required for dermatan sulfate's anticoagulant function. The increased flexibility of GalNAc(4S) ring predicted here may play a role in this, although the overall activity of these glycosaminoglycans is likely due to a complex sum of saccharide intra- and inter-residue structure, complementing interactions with heparin cofactor II.[47]

Work on elucidating the role of geometric conformation in GAGs and how it is encoded by selective chain decoration is still in its early stages.[5] This is in part due to the synthetic challenges of making point modified polysaccharides[48,49] and in part because of the difficulty in accurately simulating these highly charged compounds, both in terms of sampling its complex conformational landscape and in capturing its physical behaviour via a classical potential energy function.[5,26] The use of enhanced sampling MD methods such as the msesMD methodology afford an intuitive and efficient approach for sampling the puckering free energy

landscape of GAG monosaccharides, providing a useful route to aid our understanding of larger chain effects and to further refine the currently available models of GAG polysaccharides.

Supporting Information. Structural, energetic and error analyses of MD simulations of GAG-related monosaccharides. This material is available free of charge via the Internet at http://pubs.acs.org.

Acknowledgements

We thank Kepa Burusco for helpful discussions. This project made use of time granted via the UK High-End Computing Consortium for Biomolecular Simulation, HECBioSim (http://hecbiosim.ac.uk), supported by EPSRC (grant no. EP/L000253/1). The authors would also like to acknowledge the use of the Computational Shared Facility at the University of Manchester.

References

(1) Dwek, R. A. Glycobiology: Toward Understanding the Function of Sugars. *Chem. Rev.* **1996,** *96,* 683-720.

(2) Jackson, R. L.; Busch, S. J.; Cardin, A. D. Glycosaminoglycans: Molecular Properties, Protein Interactions, and Role in Physiological Processes. *Physiolog. Rev.* **1991,** *71,* 481-539.

(3) Bishop, J. R.; Schuksz, M.; Esko, J. D. Heparan Sulphate Proteoglycans Fine-Tune Mammalian Physiology. *Nature* **2007,** *446,* 1030.

(4) Gama, C. I.; Tully, S. E.; Sotogaku, N.; Clark, P. M.; Rawat, M.; Vaidehi, N.; Goddard III, W. A.; Nishi, A.; Hsieh-Wilson, L. C. Sulfation Patterns of Glycosaminoglycans Encode Molecular Recognition and Activity. *Nature Chem.*

Biol. **2006,** *2,* 467.

(5) Rudd, T. R.; Skidmore, M. A.; Guerrini, M.; Hricovini, M.; Powell, A. K.; Siligardi, G.; Yates, E. A. The Conformation and Structure of GAGs: Recent Progress and Perspectives. *Curr. Opin. Struct. Biol.* **2010,** *20,* 567-574.

(6) Das, S. K.; Mallet, J.; Esnault, J.; Driguez, P.; Duchaussoy, P.; Sizun, P.; Herault, J.; Herbert, J.; Petitou, M.; Sinay, P. Synthesis of Conformationally Locked L-Iduronic Acid Derivatives: Direct Evidence for a Critical Role of the Skew-Boat $^{2}S_{O}$ Conformer in the Activation of Antithrombin by Heparin. *Chem.: Eur. J.* **2001,** *7,* 4821-4834.

(7) Plazinski, W.; Drach, M. Kinetic Characteristics of Conformational Changes in the Hexopyranose Rings. *Carbohydr. Res.* **2015,** *416,* 41-50.

(8) Woods, R. J. Predicting the Structures of Glycans, Glycoproteins, and Their Complexes. *Chem. Rev.* **2018,** *118,* 8005-8024.

(9) Sattelle, B. M.; Hansen, S. U.; Gardiner, J.; Almond, A. Free Energy Landscapes of Iduronic Acid and Related Monosaccharides. *J. Am. Chem. Soc.* **2010,** *132,* 13132-13134.

(10) Naidoo, K. J. FEARCF a Multidimensional Free Energy Method for Investigating Conformational Landscapes and Chemical Reaction Mechanisms. *Sci. China Chem.* **2011,** *54,* 1962-1973.

(11) Autieri, E.; Sega, M.; Pederiva, F.; Guella, G. Puckering Free Energy of Pyranoses: A NMR and Metadynamics-Umbrella Sampling Investigation. *J. Chem. Phys.* **2010,** *133,* 09B604.

(12) Petersen, L.; Ardvol, A.; Rovira, C.; Reilly, P. J. Mechanism of Cellulose Hydrolysis by Inverting GH8 Endoglucanases: A QM/MM Metadynamics Study. *J. Phys. Chem. B* **2009,** *113,* 7331-7339.

(13) Spiwok, V.; Kralova, B.; Tvaroska, I. Modelling of α-D-Glucopyranose Ring Distortion in Different Force Fields: a Metadynamics Study. *Carbohydr. Res.* **2010,** *345,* 530-537.

(14) Babin, V.; Sagui, C. Conformational Free Energies of Methyl-α-L-Iduronic and Methyl-β-D-Glucuronic Acids in Water. *J. Chem. Phys.* **2010,** *132,* 104108.

(15) Wang, L.; Berne, B. J. Efficient Sampling of Puckering States of Monosaccharides Through Replica Exchange With Solute Tempering and Bond Softening. *J. Chem. Phys.* **2018,** *149,* 072306.

(16) Patel, D. S.; Pendrill, R.; Mallajosyula, S. S.; Widmalm, G.; MacKerell Jr, A. D. Conformational Properties of α- or β-(1-6)-Linked Oligosaccharides: Hamiltonian Replica Exchange MD Simulations and NMR Experiments. *J. Phys. Chem. B* **2014,** *118,* 2851-2871.

(17) Galvelis, R.; Re, S.; Sugita, Y. Enhanced Conformational Sampling of N-Glycans in Solution With Replica State Exchange Metadynamics. *J. Chem. Theory Comput.* **2017,** *13,* 1934-1942.

(18) Alibay, I.; Burusco, K. K.; Bruce, N. J.; Bryce, R. A. Identification of Rare Lewis Oligosaccharide Conformers in Aqueous Solution Using Enhanced Sampling Molecular Dynamics. *J. Phys. Chem. B* **2018,** *122,* 2462-2474.

(19) Atzori, A.; Bruce, N. J.; Burusco, K. K.; Wroblowski, B.; Bonnet, P.; Bryce, R. A. Exploring Protein Kinase Conformation Using Swarm-Enhanced Sampling Molecular Dynamics. *J. Chem. Inf. Model.* **2014,** *54,* 2764-2775.

(20) Burusco, K. K.; Bruce, N. J.; Alibay, I.; Bryce, R. A. Free Energy Calculations Using a Swarm-Enhanced Sampling Molecular Dynamics Approach. *Chemphyschem* **2015,** *16,* 3233-3241.

(21) Sattelle, B. M.; Almond, A. Is N-Acetyl-D-Glucosamine a Rigid $^4C_1$ Chair?

Glycobiology **2011,** *21,* 1651-1662.

(22) Hsieh, P. H.; Thieker, D. F.; Guerrini, M.; Woods, R. J.; Liu, J. Uncovering the Relationship Between Sulphation Patterns and Conformation of Iduronic Acid in Heparan Sulphate. *Sci. Rep.* **2016,** *6,* 29602.

(23) Samsonov, S. A.; Theisgen, S.; Riemer, T.; Huster, D.; Pisabarro, M. T. Glycosaminoglycan Monosaccharide Blocks Analysis by Quantum Mechanics, Molecular Dynamics, and Nuclear Magnetic Resonance. *BioMed Res. Int.* **2014,** *2014,* 808071.

(24) Case, D. A.; Babin, V.; Berryman, J. T.; Betz, R. M.; Cai, Q.; Cerutti, D. S.; Cheatham III, T. E.; Darden, T. A.; Duke, R.; Gohlke, H.; Gotz, A. W.; Gusarov, S.; Homeyer, N.; Janowski, P.; Kaus, J.; Kolassvary, I.; Kovalenko, A.; Lee, T.-S.; LeGrand, S. M.; Luchko, T.; Luo, R.; Madej, B.; Merz Jr., K. M.; Paesani, F.; Roe, D. R.; Roitberg, A.; Sagui, C.; Salomon-Ferrer, R.; Seabra, G.; Simmerling, C.; Smith, W.; Swails, J.; Walker, R. C.; Wang, J.; Wolf, R. M.; Wu, X.; Kollman, P. A. AMBER 14. 2014.

(25) Kirschner, K. N.; Yongye, A. B.; Tschampel, S. M.; González-Outeiriño, J.; Daniels, C. R.; Foley, B. L.; Woods, R. J. GLYCAM06: a Generalizable Biomolecular Force Field. Carbohydrates. *J. Comput. Chem.* **2008,** *29,* 622-655.

(26) Singh, A.; Tessier, M. B.; Pederson, K.; Wang, X.; Venot, A. P.; Boons, G. J.; Prestegard, J. H.; Woods, R. J. Extension and Validation of the GLYCAM Force Field Parameters for Modeling Glycosaminoglycans. *Can. J. Chem.* **2016,** *94,* 927-935.

(27) Jorgensen, W. L.; Chandrasekhar, J.; Madura, J. D.; Impey, R. W.; Klein, M. L. Comparison of Simple Potential Functions for Simulating Liquid Water. *J. Chem. Phys.* **1983,** *79,* 926-935.

(28) Allen, M. P.; Tildesley, D. J. *Computer Simulation of Liquids*; OUP: 1987.

(29) Lemons, D. S.; Gythiel, A. Paul Langevin's 1908 Paper "On the Theory of Brownian Motion / Sur La Theorie Du Mouvement Brownien", [CR Acad. Sci.(Paris) 146, 530-533 (1908)]. *Am. J. Phys.* **1997,** *65,* 1079-1081.

(30) Ryckaert, J. P.; Ciccotti, G.; Berendsen, H. J. C. Numerical Integration of the Cartesian Equations of Motion of a System With Constraints: Molecular Dynamics of N-Alkanes. *J. Comput. Phys.* **1977,** *23,* 327-341.

(31) Miyamoto, S.; Kollman, P. A. Settle: An Analytical Version of the SHAKE and RATTLE Algorithm for Rigid Water Models. *J. Comput. Chem.* **1992,** *13,* 952-962.

(32) Feenstra, K. A.; Hess, B.; Berendsen, H. J. Improving Efficiency of Large Time-Scale Molecular Dynamics Simulations of Hydrogen-Rich Systems. *J. Comput. Chem.* **1999,** *20,* 786-798.

(33) Hopkins, C. W.; Le Grand, S.; Walker, R. C.; Roitberg, A. E. Long-Time-Step Molecular Dynamics Through Hydrogen Mass Repartitioning. *J. Chem. Theory Comput.* **2015,** *11,* 1864-1874.

(34) Essmann, U.; Perera, L.; Berkowitz, M. L.; Darden, T.; Lee, H.; Pedersen, L. G. A Smooth Particle Mesh Ewald Method. *J. Chem. Phys.* **1995,** *103,* 8577-8593.

(35) Darden, T.; York, D. M.; Pedersen, L. Particle Mesh Ewald: An N.Log(N) Method for Ewald Sums in Large Systems. *J. Chem. Phys.* **1993,** *98,* 10089-10092.

(36) Hill, A. D.; Reilly, P. J. Puckering Coordinates of Monocyclic Rings by Triangular Decomposition. *J. Chem. Inf. Model.* **2007,** *47,* 1031-1035.

(37) Cremer, D.; Pople, J. A. General Definition of Ring Puckering Coordinates. *J. Am. Chem. Soc.* **1975,** *97,* 1354-1358.

(38) Meirovitch, H. Recent Developments in Methodologies for Calculating the Entropy and Free Energy of Biological Systems by Computer Simulation. *Curr. Opin. Struct.*

Biol. **2007,** *17,* 181-186.

(39) Torrie, G. M.; Valleau, J. P. Nonphysical Sampling Distributions in Monte Carlo Free-Energy Estimation: Umbrella Sampling. *J. Comput. Phys.* **1977,** *23,* 187-199.

(40) Roe, D. R.; Cheatham, T. E. PTRAJ and CPPTRAJ: Software for Processing and Analysis of Molecular Dynamics Trajectory Data. *J. Chem. Theory Comput.* **2013,** *9,* 3084-3095.

(41) Plazinski, W.; Drach, M. The Dynamics of the Conformational Changes in the Hexopyranose Ring: a Transition Path Sampling Approach. *RSC Adv.* **2014,** *4,* 25028-25039.

(42) Lins, R. D.; Hunenberger, P. H. A New GROMOS Force Field for Hexopyranose-Based Carbohydrates. *J. Comput. Chem.* **2005,** *26,* 1400-1412.

(43) Harder, E.; Damm, W.; Maple, J.; Wu, C.; Reboul, M.; Xiang, J. Y.; Wang, L.; Lupyan, D.; Dahlgren, M. K.; Knight, J. L.; Kaus, J. W.; Cerutti, D. S.; Krilov, G.; Jorgensen, W. L.; Abel, R.; Friesner, R. A. OPLS3: A Force Field Providing Broad Coverage of Drug-Like Small Molecules and Proteins. *J. Chem. Theory Comput.* **2016,** *12,* 281-296.

(44) Guerrini, M.; Elli, S.; Mourier, P.; Rudd, T. R.; Gaudesi, D.; Casu, B.; Boudier, C.; Torri, G.; Viskov, C. An Unusual Antithrombin-Binding Heparin Octasaccharide With an Additional 3-O-Sulfated Glucosamine in the Active Pentasaccharide Sequence. *Biochem. J.* **2013,** *449,* 343-351.

(45) Hricovini, M.; Guerrini, M.; Bisio, A.; Torri, G.; Petitou; Benito, C. A. S. U. Conformation of Heparin Pentasaccharide Bound to Antithrombin III. *Biochem. J.* **2001,** *359,* 265-272.

(46) Sattelle, B. M.; Almond, A. Assigning Kinetic 3D-Signatures to Glycocodes. *Phys. Chem. Chem. Phys.* **2012,** *14,* 5843-5848.

(47) Pavao, M. S.; Mourao, P. A.; Mulloy, B.; Tollefsen, D. M. A Unique Dermatan Sulfate-Like Glycosaminoglycan From Ascidian: Its Structure and the Effect of Its Unusual Sulfation Pattern on Anticoagulant Activity. *J. Biol. Chem.* **1995,** *270,* 31027-31036.

(48) Jayson, G. C.; Miller, G. J.; Hansen, S. U.; Barath, M.; Gardiner, J. M.; Avizienyte, E. The Development of Anti-angiogenic Heparan Sulfate Oligosaccharides. *Biochem. Soc. Trans*. **2014**, 42, 1596-1600.

(49) Hansen, S. U.; Miller, G. J.; Jayson, G. C.; Gardiner, J. M. First Gram-Scale Synthesis of a Heparin-Related Dodecasaccharide. *Org. Lett.* **2012,** *15,* 88-91.

Figure captions

Figure 1 Monosaccharides α-D-glucose (α-Glc), β-D-glucose (β-Glc), α-L-iduronic acid (α-Glc), β-D-glucuronic acid (β-GlcA); glycosaminoglycan monosaccharides GlcNAc and GalNAc and their sulfated variants

Figure 2 Free energy profiles as a function of Cremer-Pople puckering angle θ for (a) α-Glc, (b) β-Glu, (c) IdoA and (d) GlcA calculated via unbiased MD trajectories of varying length or via 195 ns msesMD simulations. Energies in kcal/mol.

Figure 3 Time series of Cremer-Pople θ angle computed from respective 20 μs MD and 195 ns msesMD simulations of (a,b) α-Glc, (c,d) β-Glu, (e,f) IdoA and (g,h) GlcA

Figure 4 Evaluation of the convergence of free energy profile computed via 195 ns msesMD as a function of Cremer-Pople puckering angle θ for (a) α-Glc, (b) β-Glu, (c) IdoA and (d) GlcA

Figure 5 Free energy profiles as a function of Cremer-Pople puckering angles θf computed from respective 20 μs MD and 195 ns msesMD simulations of (a,b) α-Glc, (c,d) β-Glu, (e,f) IdoA and (g,h) GlcA

Figure 6 Free energy profiles as a function of Cremer-Pople angle θ evaluating the impact of ring modification of (a) IdoA, (b) GlcA, (c) GlcNAc and (d) GalNAc, computed from 195 ns msesMD simulations.

Figure 7 Free energy profiles as a function of Cremer-Pople puckering angles θϕ from 195 ns msesMD simulation of (a) IdoA, (b) IdoA2S, (c) GlcA, (d) GlcA2S, (e) GlcNAc, (f) GlcNS, (g) GlcNS(3S), (h) GlcNAc(6S), (i) GlcNAc(3S,6S), (j) GalNAc, (k) GalNAc(4S), (l) GalNAc(6S) and (m) GalNAc(4S,6S).

Figure 8 (a) Selected conformations of $^{1}C_{4}$ conformers of (a) GalNAc(4S) and (b) GalNAc(4S,6S) indicating the type of intra-molecular hydrogen bond pattern which can be accessed (with representative distances in Å)

Table 1 Relative free energy of $^{1}C_{4}$ and selected non-chair conformers (lying within 0.5 kcal/mol of the lowest energy non-chair conformer) of monosaccharides relative to $^{4}C_{1}$ chair form (kcal/mol), computed via MD and 195 ns msesMD simulations.

Residue	$^{1}C_{4}$		Non-chair	
	MD	msesMD	MD	msesMD
α-Glc	0.2	0.2	$^{1}S_{5}$ [2.9], $B_{2,5}$ [3.0]	$^{1}S_{5}$ [2.4]
β-Glc	3.5	3.3	$^{1}S_{3}$ [3.1], $^{1,4}B$ [3.2], $^{O}S_{2}$ [3.3], $^{3}S_{1}$ [3.2], $^{3}B_{O}$ [3.5]	$^{1}S_{3}$ [3.2], $^{O}S_{2}$ [3.3], $^{3}S_{1}$ [3.4], $^{1,4}B$ [3.5], $^{1}S_{5}$ [3.6], $^{2}S_{O}$ [3.7]
IdoA	-0.3	-0.5	$^{2}S_{O}$ [1.5], $^{3}S_{1}$ [1.7], $B_{1,4}$ [1.9]	$^{2}S_{O}$ [1.6], $^{3}S_{1}$ [1.8], $B_{1,4}$ [2.0]
GlcA	2.8	3.2	$^{1}S_{3}$ [2.1], $B_{3,O}$ [2.4]	$^{1}S_{3}$ [2.2], $B_{3,O}$ [2.5]

Table 2 Relative free energy of $^{1}C_4$ and selected non-chair conformers (lying within 0.5 kcal mol^{-1} of the lowest energy non-chair conformer) of monosaccharides relative to $^{4}C_1$ chair form (kcal/mol), computed via 195 ns msesMD simulations.

Residue	**$^{1}C_4$**	**Non-chair**
IdoA(2S)	0.2	$^{3}S_1$ [1.1], $^{2}S_O$ [1.3], $B_{1,4}$ [1.4]
GlcA(2S)	2.6	$^{1}S_3$ [2.0], $B_{3,O}$ [2.2]
GlcNAc	1.4	$B_{3,O}$ [4.0], $^{1}S_3$ [4.1], $^{2}S_O$ [4.2], $^{1,4}B$ [4.3]
GlcNS	1.9	$^{1}S_3$ [4.0], $^{1}S_5$ [4.1], $B_{3,O}$ [4.2], $^{1,4}B$ [4.3], $^{2}S_O$ [4.4]
GlcNS(3S)	1.8	$^{O}S_2$ [3.8], $^{1}S_5$ [4.0], $B_{3,O}$ [4.1], $^{2}S_O$ [4.1], $^{1,4}B$ [4.2], $B_{2,5}$ [4.3]
GlcNS(6S)	1.3	$^{1}S_3$ [3.9], $^{1}S_5$ [4.0], $B_{3,O}$ [4.1], $^{2}S_O$ [4.2], $^{1,4}B$ [4.2]
GlcNS(3S,6S)	1.6	$^{2}S_O$ [3.9], $B_{3,O}$ [3.9], $^{O}S_2$ [4.1], $B_{2,5}$ [4.3]
GalNAc	N/A	$^{1}S_3$ [4.4]
GalNAc(4S)	5.0	$^{1}S_3$ [3.9]
GalNAc(6S)	N/A	$^{1}S_3$ [4.4]
GalNAc(4S,6S)	8.3	$^{1}S_3$ [3.5]

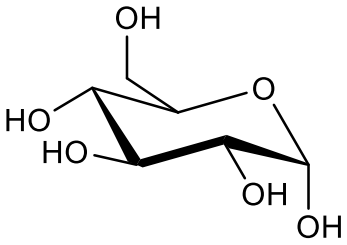

α-D-Glc

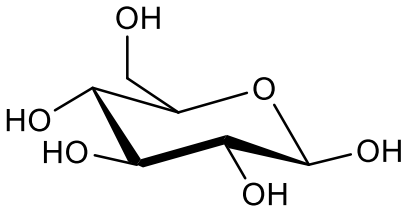

β-D-Glc

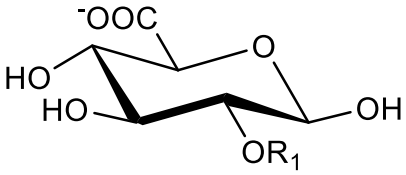

β-D-GlcA

R_1: H or SO_3^-

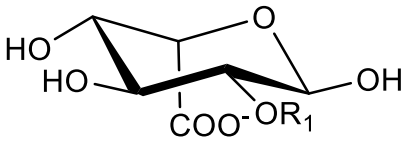

α-L-IdoA

R_1: H or SO_3^-

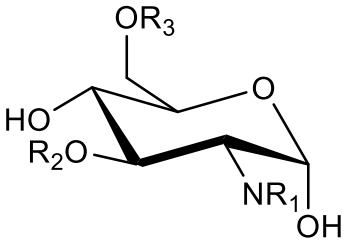

α-D-Glc

R_1: Ac, SO_3^-

R_2,R_3: H or SO_3^-

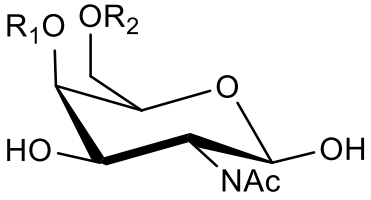

β-D-GalNAc

R_1,R_2: H or SO_3^-

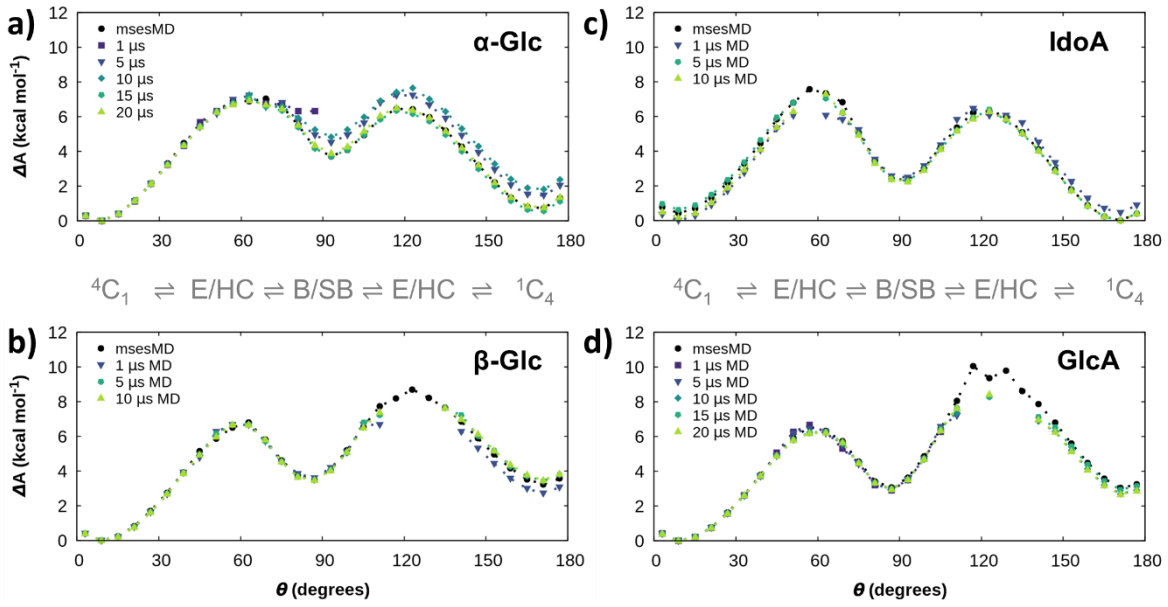
a)
α-Glc
msesMD
1 µs
5 µs
10 µs
15 µs
20 µs
ΔA (kcal mol-1)
4C1 ⇌ E/HC ⇌ B/SB ⇌ E/HC ⇌ 1C4
c)
IdoA
msesMD
1 µs MD
5 µs MD
10 µs MD
4C1 ⇌ E/HC ⇌ B/SB ⇌ E/HC ⇌ 1C4
b)
β-Glc
msesMD
1 µs MD
5 µs MD
10 µs MD
ΔA (kcal mol-1)
θ (degrees)
d)
GlcA
msesMD
1 µs MD
5 µs MD
10 µs MD
15 µs MD
20 µs MD
θ (degrees)

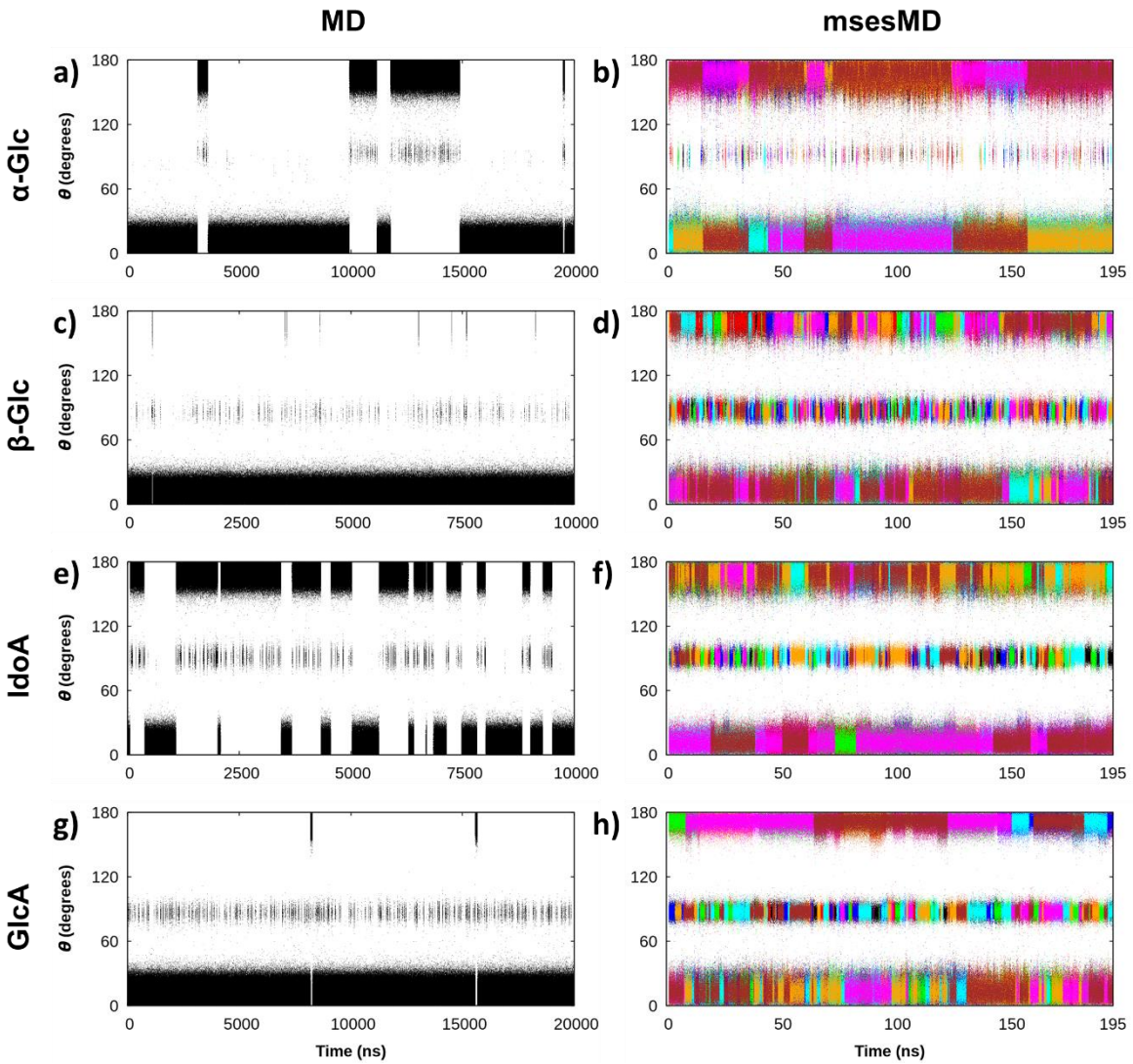
MD
msesMD
a)
b)
c)
d)
e)
f)
g)
h)
α-Glc
β-Glc
IdoA
GlcA
θ (degrees)
Time (ns)
0
60
120
180
0
5000
10000
15000
20000
2500
7500
50
100
150
195

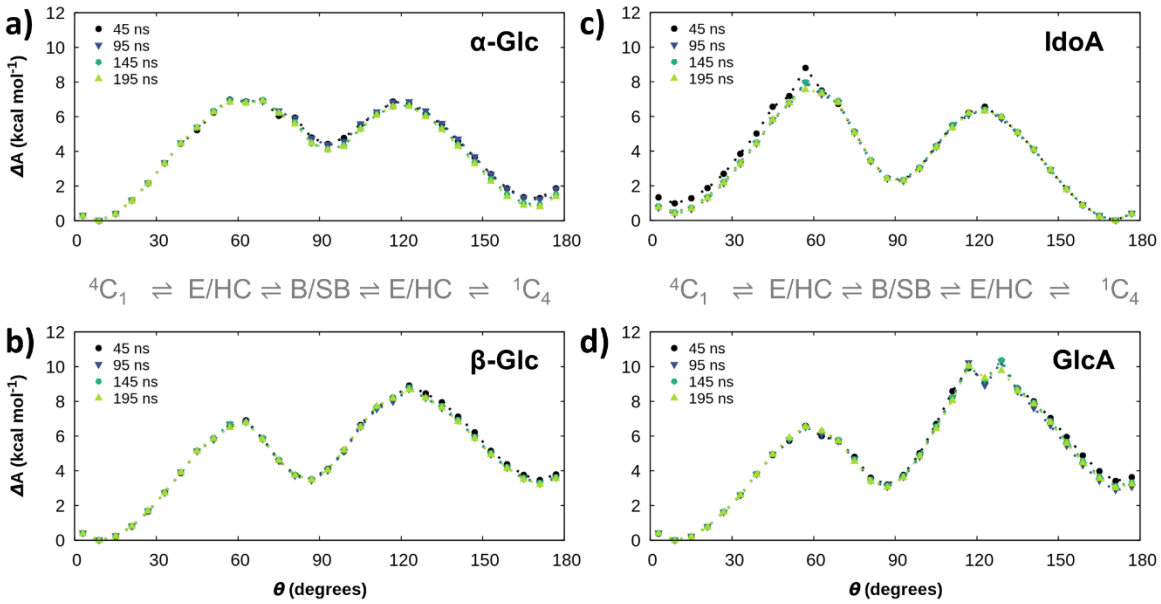
a)
α-Glc
45 ns
95 ns
145 ns
195 ns
ΔA (kcal mol-1)
4C1 ⇌ E/HC ⇌ B/SB ⇌ E/HC ⇌ 1C4
c)
IdoA
45 ns
95 ns
145 ns
195 ns
4C1 ⇌ E/HC ⇌ B/SB ⇌ E/HC ⇌ 1C4
b)
β-Glc
45 ns
95 ns
145 ns
195 ns
ΔA (kcal mol-1)
θ (degrees)
d)
GlcA
45 ns
95 ns
145 ns
195 ns
θ (degrees)

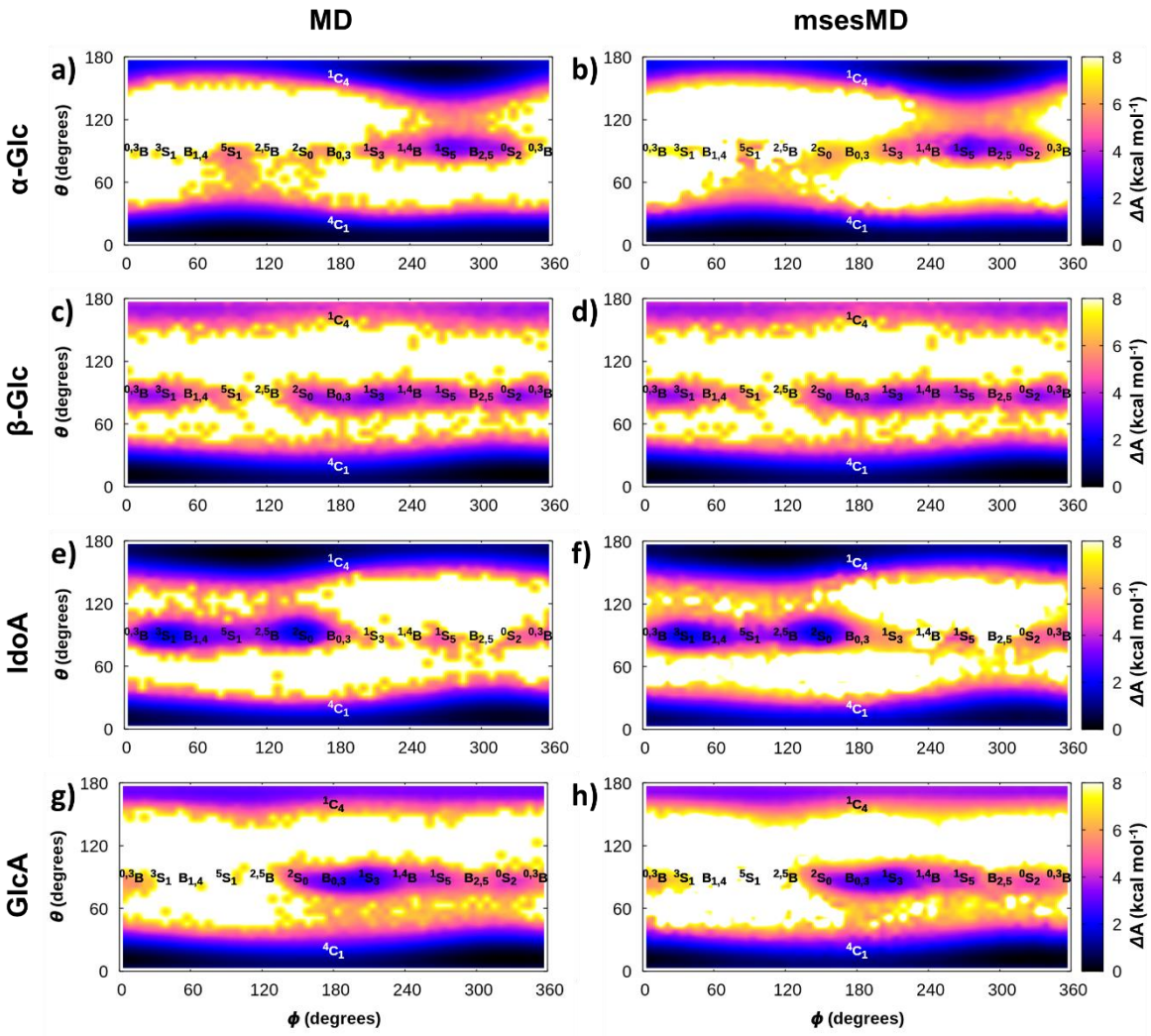
MD
msesMD
α-Glc
β-Glc
IdoA
GlcA
a)
b)
c)
d)
e)
f)
g)
h)
θ (degrees)
ϕ (degrees)
ΔA (kcal mol⁻¹)
1C4
4C1
0,3B 3S1 B1,4 5S1 2,5B 2S0 B0,3 1S3 1,4B 1S5 B2,5 0S2 0,3B

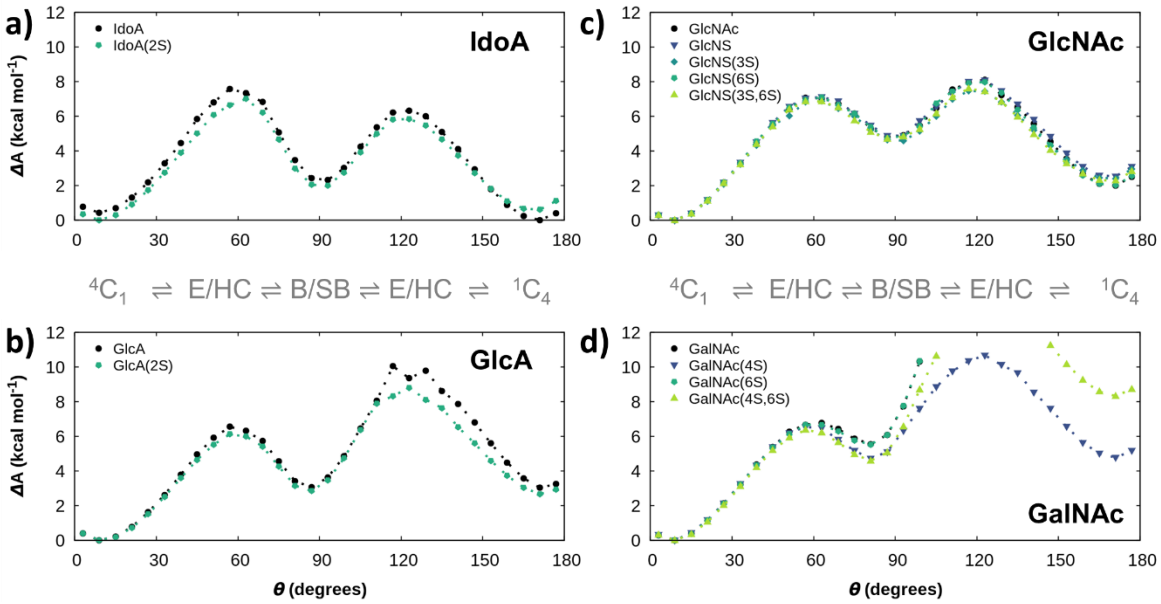
a)
IdoA
IdoA(2S)
IdoA
ΔA (kcal mol-1)
4C1 ⇌ E/HC ⇌ B/SB ⇌ E/HC ⇌ 1C4
c)
GlcNAc
GlcNS
GlcNS(3S)
GlcNS(6S)
GlcNS(3S,6S)
GlcNAc
4C1 ⇌ E/HC ⇌ B/SB ⇌ E/HC ⇌ 1C4
b)
GlcA
GlcA(2S)
GlcA
ΔA (kcal mol-1)
θ (degrees)
d)
GalNAc
GalNAc(4S)
GalNAc(6S)
GalNAc(4S,6S)
GalNAc
θ (degrees)

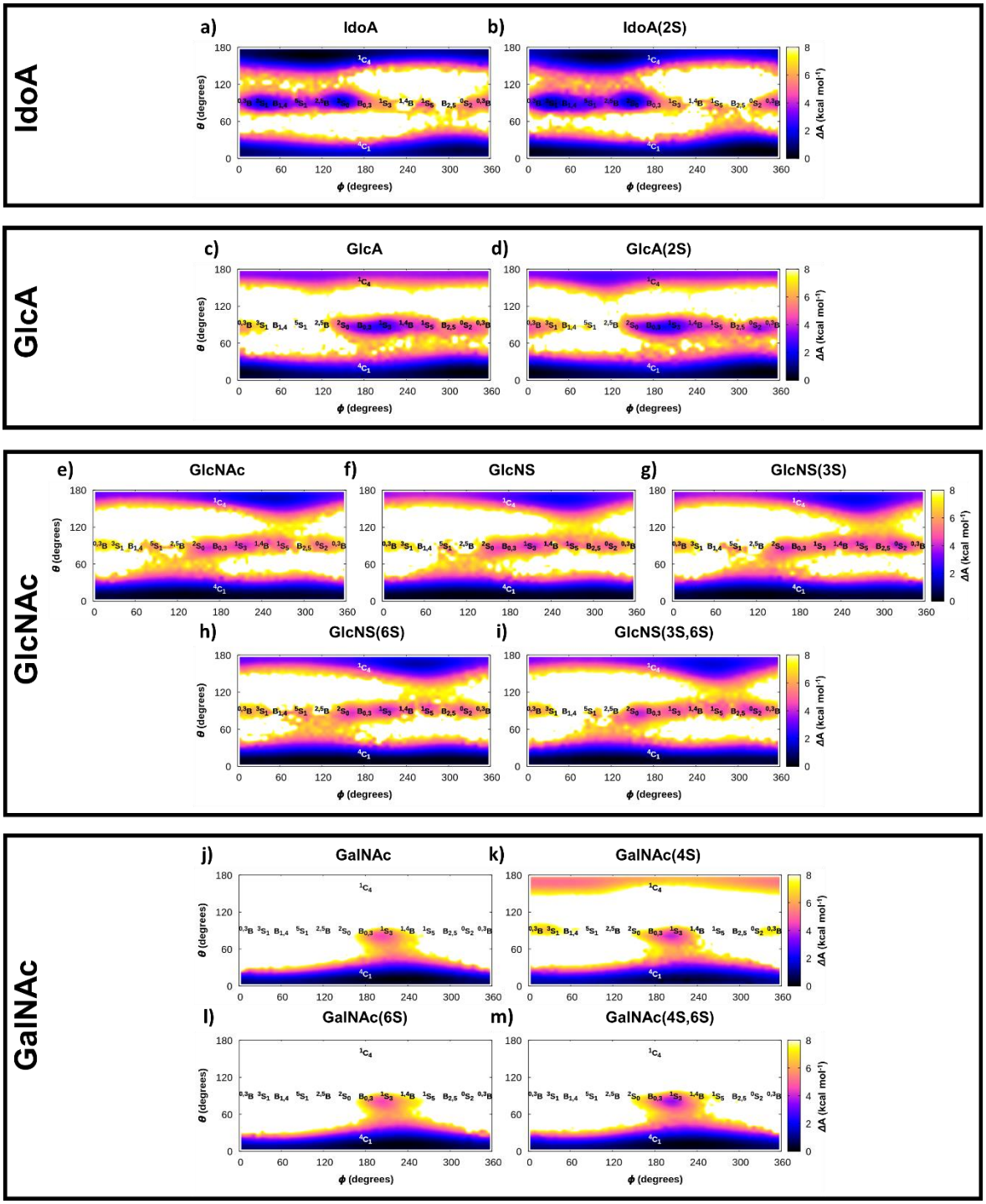
IdoA
a)
IdoA
b)
IdoA(2S)
GlcA
c)
GlcA
d)
GlcA(2S)
GlcNAc
e)
GlcNAc
f)
GlcNS
g)
GlcNS(3S)
h)
GlcNS(6S)
i)
GlcNS(3S,6S)
GalNAc
j)
GalNAc
k)
GalNAc(4S)
l)
GalNAc(6S)
m)
GalNAc(4S,6S)
θ (degrees)
ϕ (degrees)
ΔA (kcal mol⁻¹)

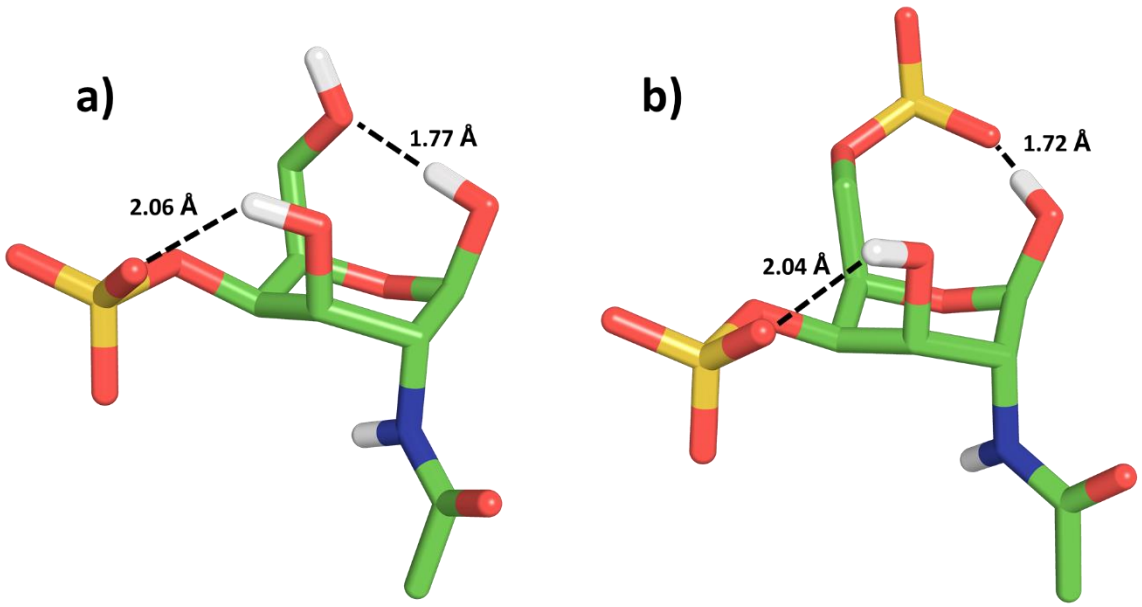
a)
1.77 Å
2.06 Å
b)
1.72 Å
2.04 Å